Tubular Membrane Electrode Assembly for PEM electrolysis

A.Laube[a,b,*], A.Hofer[c], B.Sánchez Batalla[e], S.Ressel[a], A.Chica[b], S.Fischer[f], C.Weidlich[e], J.Bachmann[c,d], T.Struckmann[a]

[a] *Hamburg University of Applied Sciences, Department of Mechanical Engineering and Production Management, Berliner Tor 21, 20099, Hamburg, Germany*
[b] *Instituto de Tecnología Química, Universitat Politecnica de Valenciad-Consejo Superior de Investigaciones Científicas, Avenida de los Naranjos s/n, 46022, Valencia, Spain*
[c] *Friedrich-Alexander University of Erlangen-Nuernberg, Department of Chemistry and Pharmacy, Chemistry of Thin Film Materials, IZNF/Cauerstr. 3, 91058 Erlangen, Germany*
[d] *Saint-Petersburg State University, Institute of Chemistry, Universitetskii pr. 26, 198504 St. Petersburg, Russia*
[e] *DECHEMA Research Institute,Applied Electrochemistry, Theodor-Heuss-Allee 25,60486 Frankfurt am Main, Germany*
[f] *UNIWELL Rohrsysteme GmbH, Siegelfelder Straße 1, 96106 Ebern, Germany*

Abstract

Polymer electrolyte membrane (PEM) water electrolysis is already widely used for hydrogen production but still needs further cost reductions. While tubular cell designs might reduce production costs by extrusion production of cell components and small sealing lengths, catalyst coating methods like atomic layer deposition (ALD) might reduce catalyst costs significantly. This study demonstrates the feasibility of a tubular PEM electrolyzer membrane electrode assembly (MEA) for the oxygen half cell with 5.0 mm diameter. An extruded perfluorosulfonic acid (PFSA) cation exchange membrane is combined with a porous transport electrode (PTE) consisting of a titanium felt with low a iridium catalyst loading obtained by ALD. The performance is experimentally characterized in a complete tubular cell setup by polarization curve and ohmic resistance measurements. Operation in sulphuric acid at a cell voltage of 1.7 V and a cell temperature of 60°C results in an overall current density of 55 mA/cm^2 and an iridium mass activity > 680 A/g which is up to 3 times larger than liter-

*Corresponding author. E-mail address: armin.laube@haw-hamburg.de (A.Laube).

ature values. The high frequency ohmic resistance of the cell turns out to be 0.96 Ωcm^2. By this way and up to the knowledge of the authors, a tubular PEM electrolysis cell is designed, assembled and characterized for the first time.
Keywords: cylindric cell design, PEM water electrolysis, ALD catalyst coating, porous transport electrodes

1. Introduction

Hydrogen production by water electrolysis is a key element in the energy transition process for achieving deep decarbonization [1, 2, 3]. In particular (PEM) electrolysis using proton exchange membranes (reactions in 1) is currently widely studied since it offers advantages over the established alkaline electrolysis due to a reduced overpotential and a faster response to dynamic power changes.

Overall reaction:

$$2H_2O \rightarrow 2H_2 + O_2 \tag{1}$$

Anode (OER: oxygen evolution reaction):

$$2H_2O \rightarrow O_2 + 4H^+ + 4e^- \tag{2}$$

Cathode (HER: hydrogen evolution reaction):

$$4H^+ + 4e^- \rightarrow 2H_2 \tag{3}$$

The cost challenges of PEM electrolysis are the catalyst costs for platinum group metals with about 10-20% and high cell assembly costs with about 12% of the whole stack costs [4, 5, 6]. Commercial PEM electrolysis cells feature a planar cell design. They usually combine bipolar titanium plates as current collectors with integrated flow channels, porous transport layers like graphite felts or carbon papers in the cathode half cell and sintered titanium felts, felts or plates in the anode half cell with a catalyst coated polymer electrolyte membrane made of PFSA material. Their typical catalyst loadings are $(0.5 - 1)\ mg/cm^2$

platinum for the cathode and $(1.5 - 2.5)$ mg/cm^2 iridium or ruthenium (oxides) for the anode [7, 8, 9, 10]. Though the research on this conventional cell and catalyst coating setup show continuous progress [11], new cell and catalyst concepts are investigated and might be needed for further significant cost reduction[12].

Several approaches for catalyst loading reductions have been proposed [13, 14, 15, 16, 17]. Among them, catalyst coating by atomic layer deposition (ALD) has turned out to be a promising candidate to achieve catalyst loadings in the 0.1 mg/cm^2 range [18, 19, 20, 21, 22, 23]. This coating technique deposits the catalyst layer on the porous transport layer and thus leads to porous transport electrodes. The research focus is often on the anode catalyst since the oxygen evolution reaction (OER) is the limiting reaction and iridium exhibits limited availability due to mining capacities, nevertheless cathodic platinum loading reduction is desirable as well.

Significant steps towards lower production and assembly costs would be the reduction of sealing lengths and the extrusion production of cell components. Using a tubular cell setup, both targets and additionally a higher stability against half cell pressure differences can be accomplished. Furthermore, a reduction of the reactor dimensions and costs has been identified for tubular solid oxid fuel cells compared to the planar design[24]. While the tubular setup is already partly used in solid oxide fuel cells [25, 26, 27, 28, 3, 29], PEM fuel cells [30, 31, 32, 33, 34] and direct methanol fuel cells [35, 36], the feasibility of tubular energy conversion cells with extruded cell components, tubular membranes and current collectors with flow fields, has only been demonstrated for all vanadium and vanadium air redox flow cells [37, 38, 39].

This study combines both approaches, the tubular geometry and ALD, and investigates the feasibility of an anodic, tubular MEA with an extruded polymer exchange membrane and an ALD iridium coated and rolled titanium felt as a porous transport electrode. The MEA performance is studied in a complete cell setup using an ALD platinum coated graphite felt and a titanium current collector with integrated flow fields for cathode half cell.

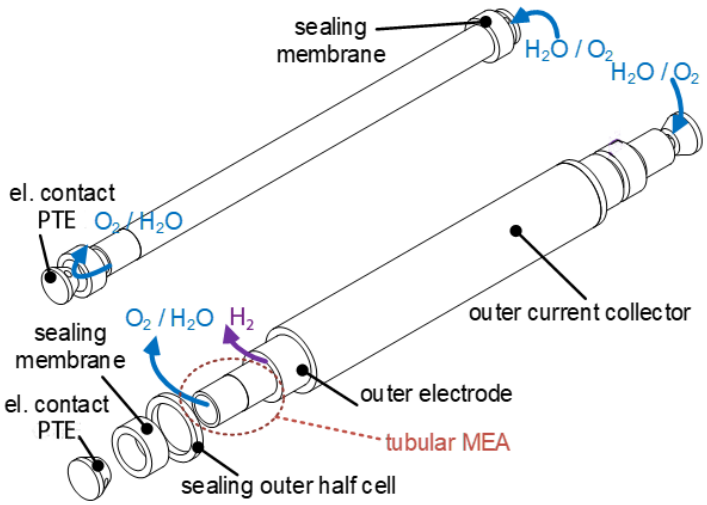

Figure 1: Top: Tubular MEA with sealing and connection. Bottom: The complete tubular cell

2. Experimental

2.1. Tubular cell design

Analogue to the planar cell design, the anode, cathode and membrane form the the tubular PEM electrolysis cell. The arrangement however is concentric, a tubular membrane separates the inner from the outer half cells as shown in figure 1. While the outer half cell can be handle similar to planar cells, the tubular geometry implies constraints concerning catalyst application and electrical connection for the inner half cell. The electrical current needs to be conducted towards the electrical connection at the ends of the cell. In PEM electrolysis cells, highly conductive titanium and titanium alloys are commonly used for the OER in the anodic half cell due to the high overpotentials while less conductive graphite materials are commonly used for the cathode half cell. Therefore, the anode half cell will be considered for the inner half cell. For an inline production by co-extrusion, which fabricates an endless MEA, established catalyst application methods such as spray or blade coating on the membrane need a high effort and are hardly applicable. However, a PTE approach, with

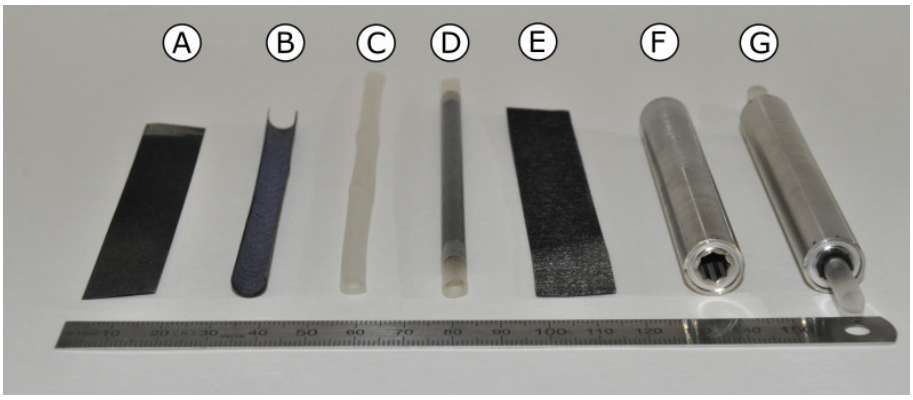

Figure 2: Cell components and fabrication steps; A: Anode PTE; B: Pre-rolled anode PTE; C: Tubular Membrane; D: Tubular MEA; E: Cathode PTE; F: Titanium current collector; G: Assembled tubular PEM electrolysis cell.

a separate catalyst application onto the porous transport layer, enables the inline production by co-extrusion. Therefore the PTE approach, which has been previously demonstrated in a planar cell design [23], has been selected for the tubular PEM electrolysis cell for the anode and cathode half cell.

Figure 2 exhibits the components of the cell body in different fabrication stages. The order from left to right corresponds to the order from the inside to the outside in the tubular geometry. The anode PTE substrate (A) is a titanium felt from Baekert (ST/Ti/20/350/50) with a thickness of 160 μm, a fiber diameter of 20 μm and a porosity of 50 %. In this work, the pre-rolled anode PTE (B) and the tubular membrane (C) form the MEA (D). The tubular MEA has an inner membrane diameter of 5 mm, an active length of 100 mm and thereby an active membrane surface area of 15.7 mm^2. The total length of the tubular MEA is extended by 8 mm on each end for the sealing and the electrical connection. The tubular MEA is enclosed by the cathode PTE (E), a thermally activated and ALD platinum coated graphite felt (Sigracet ECM 130, SGL Carbon). The outer, cathode half cell is enclosed by a custom made titanium grade 2 current collector(F) with an inner diameter of 6.2 mm and 8 equally spaced, straight flow channels on the circumference. While in planar

cells the force, which is needed to connect the components electrically, can be achieved by an outer clamping force, the electrical connection in tubular cells can be achieved by the geometrical compression of the PTE. The cathode PTE is compressed from 950 μm to 500 μm which corresponds to a compression rate of 47 %. A titanium grade 2 cone is pressed into one end of the MEA for the electrical connection and additionally serves as the product outlet of the inner, anode half cell. The tubular cell (G) is enclosed by two identical PVDF end plates with integrated manifolds. Both half cells are sealed between the half cells and the end plates with O-ring sealings and against each other with a potting compound at the end of the tubular MEA.

2.2. Electrode preparation

The anode electrode is anodized and coated with iridium by ALD as described by Hofer et al. [22]. Prior to the catalyst coating, the titanium felt of the anode PTE was pretreated with anodization to create a nano structured surface and thereby enlarge the active area. For planar cells an active area increase by a factor of $200-500$ depending on the diameter and length of the nano pores was determined [40]. A nominal iridium layer thickness of 7.2 nm (100 coating cycles) was determined on silicon wafers by spectroscopic ellipsometry with a SENPro from SEN-TECH. In a previous publication of the authors [23], PTEs have been fabricated using the same procedure but with 150 ALD cycles resulting in an iridium loading of 120 $\mu g/cm^2$ as measured with ICP-MS. For 100 ALD cycles we thus conclude an iridium loading of 80 $\mu g/cm^2$ for the tubular anode PTE. A graphite felt (Sigracet ECM 130, SGL Carbon) serves as the substrate for the cathode PTE. The felt was heat treated for 3 hours at $450°C$ and coated with platinum by ALD following the procedure of previously tested planar cells with PTEs[23]. Platinum was deposited in 30 cycles on the activated graphite felt. This corresponds to a nominal thickness on silicon wafers of approximately 2 nm and a platinum loading of 0.28 mg/cm^2 as measured with ICP-MS.

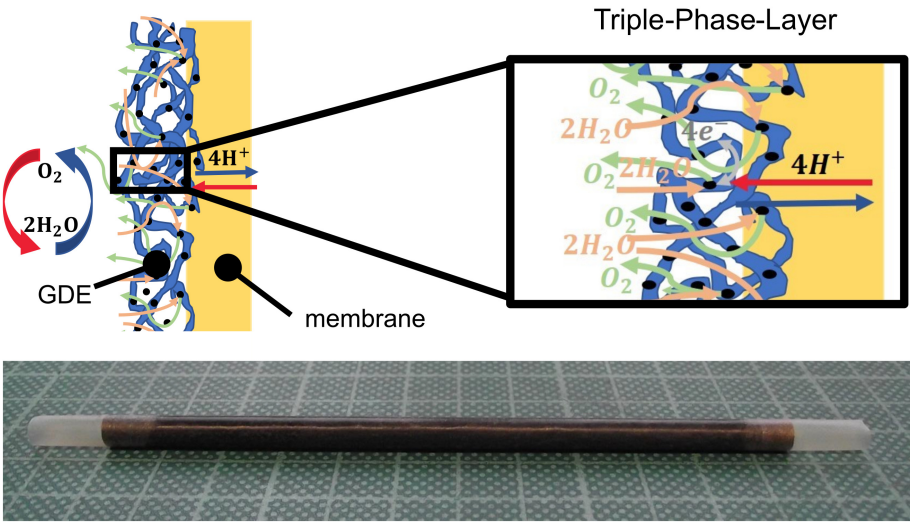

Figure 3: (Top) Charge and mass transfer in the three phase layer of a PTE-MEA; (bottom) the tubular MEA after heat bonding

2.3. Tubular MEA fabrication

The tubular cation exchange membrane is manufactured by extrusion (Uniwell GmbH & Co KG) of perflouronated sulfonic acid/PTFE copolymer granulate material VM fumasep FFT of FUMATECH BWT as described in [39]. The tubular membrane has an inner diameter of 5.0 mm and a wall thickness of 90 μm. An in-plane conductivity of $> 90\ mS/cm$ was measured in demineralized H_2O with the 4 electrode setup 'MK3' of FUMATECH BWT.

In order to increase the three phase layer of the ALD PTE and to facilitate ionic conductivity across the electrode thickness, the tubular membrane and PTE are heat bonded as schematically shown in the top of figure 3. In the first step, the planar PTE sheets were pre-rolled to the tubular shape in longitudinal direction. The tubular membranes were hydrated for 1 h in deionised water and were then slipped over the rolled PTE. For the heat bonding process, a titanium pin with a length of 170 mm was inserted in the loose MEA. The MEA components and titanium pin were pressed into an outer tubular PTFE pipe. The compression of the PTE and the membrane was defined by the

clearance of the PTFE pipe and the titanium pin. The heat input was achieved by Joule heating of the titanium pin and defined by the applied current and time. A uniform heat input across the entire PTE surface area was reached and is shown in figure 3 (darker part in the middle of the MEA). The membrane material penetrates deep into the titanium fibres of the PTE while no titanium fibre stitches through the tubular membrane. Thereby, the three phase layer is increased and the PTE and membrane are fixed to a tubular MEA to enable the cell assembly process.

2.4. Electrochemical Testing

For the electrochemical characterization a potentiostat SP150 in combination with a VMP3 Booster from Biologic was used in a test rig as described in [23]. The electrolyte flow rate was set to 10 ml/min with a peristaltic pump (Masterflex). All characterisations were performed at ambient pressure and at a temperature of 60°C by using heat plates(CAT-m2021) and temperature sensors in the tanks, fluid cycles and the test cell housing. The test routine consisted of a membrane break in phase, a heat up phase and the electrochemical characterization. During the membrane break in, a voltage of 1.6 V was applied for two hours. The heat up took two hours, while the temperature was nearly constant after one hour. The techniques used for the electrochemical characterization were polarisation curves (PC) by linear sweep voltammetry (LSV), electrochemical impedance spectroscopy (EIS), current interrupt (CI) and chronoamperometry (CA) measurements. The PCs were recorded by a linear voltage sweep with slope 20 mV/min from 1.2 V to 1.7 V. EIS and CI measurements were performed to investigate the area specific cell resistance (ASR). EIS measurements were done in galvanostatic operation with average current density 15 mA/cm^2 and a 1.5 mA/cm^2 amplitude. The CI measurements were done with three repetitions using an applied current of 15 mA/cm^2 which was held for 0.5 s, followed by a relaxing time of 5 s with a sampling rate of $2,500$ Hz. The cell voltage of all characterization methods was limited to 1.7 V in order to avoid degradation effects during characterizations. For

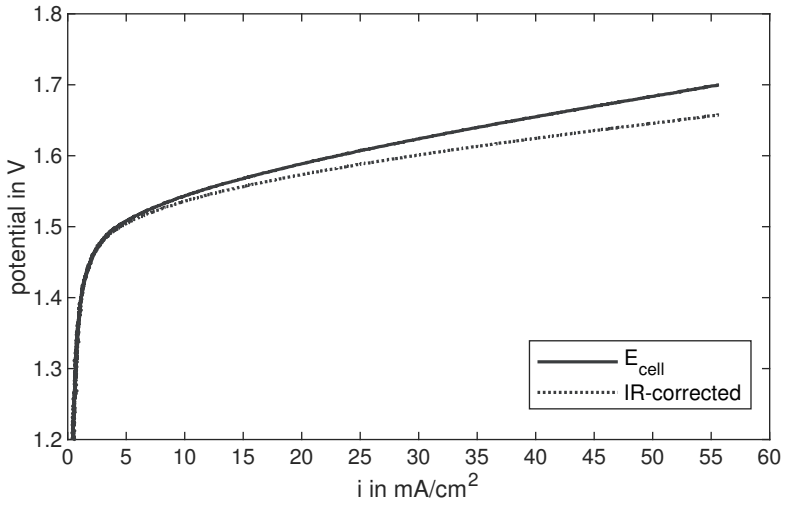

Figure 4: Polarisation curve analysis of the cell potential and IR correctd cell potential

the CA measurements, constant voltage was applied in 0.1 V steps from 1.2 V (theoretical OCV) to 1.7 V, holding each step for $2h$. At each voltage step, the mean value of the current over the last hour was determined for validating the PC data recorded with LSV. The cell is operated with 1 mol/l sulphuric acid in both half cells to achieve a sufficiently high protonic conductivity for the whole catalyst coated area.

3. Results and Discussion

The leak tightness of the test cell was tested before operating the tubular PEM electrolysis cell. The cell was filled with argon and a pressure of 100 mbar was applied on each half cell for 24 h without observing any leakage. Additionally, over the entire characterisation and after 6 months of storage in 1 mol/l sulphuric acid, the cell shows no failure of the sealings.

The test cell performance is analysed by the LSV polarization curve taken after the membrane break in and heat up phases as shown in figure 4. The maximum current density of 55 mA/cm^2 is not far from current densities of planar PTE cells with comparable catalyst loadings [23] but well below cur-

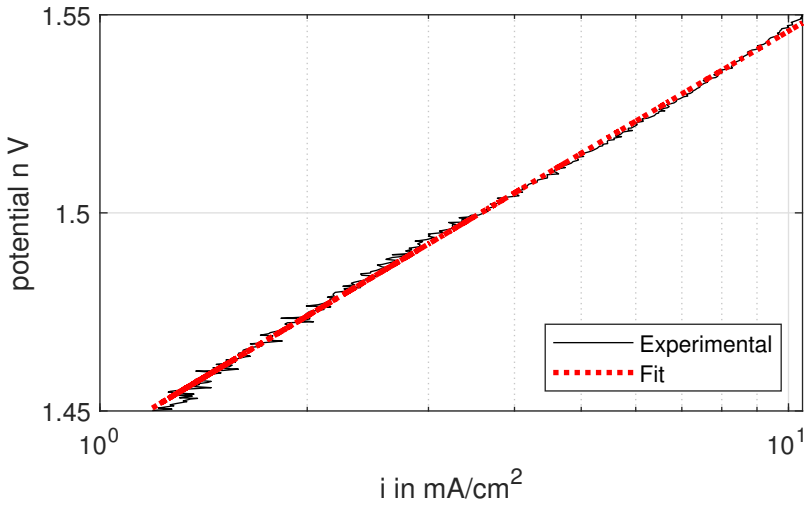

Figure 5: Tafel-plot of the polarization curve and ASR fit with 4

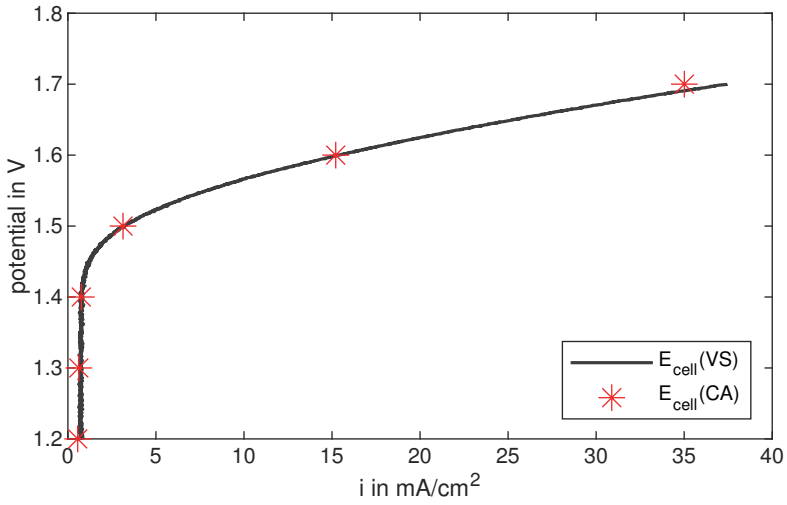

Figure 6: Polarisation curve recorded with linear sweep voltammetry (VS) and chronoamperometry (CA) steps

rent densities of cells using the commercial catalyst coated membrane (CCM) approach at the same conditions[41, 42, 43, 44, 45]. Since the ALD PTE cell operates with very low catalyst loadings, we consider the corresponding mass activities as defined by the current to catalyst mass ratio of iridium. The tubular cell reached a mass activity of $> 680\ A/g_{Ir}$ which is well above published data for standard CCM cells ($245 - 500\ A/g_{Ir}$) and comparable to planar PTE cell values [42, 43, 41, 44, 45].

As ohmic contributions to the total overpotential are usually significant, the dotted line in figure 5 shows the iR-free polarization curve of the cell. iR-correction was performed by subtracting the ohmic overpotential using the area specific resistances ASR_{EIS} from galvanostatic EIS measurements. At the maximum current density the iR-free overpotential is about 10 % below the overall overpotential for $E_0 = 1.2\ V$ vs. standard hydrogen electrode potential at 60 $^{\circ}C$. At low current densities, the iR-free potential can be solely attributed to the dominating activation overpotential.

The Tafel plot of iR-free polarization curve from 1.45 V to 1.55 V cell potential $E(i)$ is shown in figure 5. Experimental data are fitted according to the Tafel equation

$$E(i) - E_0 = b \cdot ln(i/i_0) \tag{4}$$

using the fit parameters exchange current density i_0 and Tafel slope b (red curve). Compared to previously published PTE cell data [23] the Tafel slope is almost doubled ($100\ mV/dec$) while i_0 exhibits the same order of magnitude ($0.005\ mA/cm^2$). These results are in line with the increased activation overpotential in the polarization curve compared with commercial CCM cells observed for planar PTE cells[23].

Figure 6 finally compares the LSV polarization curve data after CA (black curve) and the average current densities in the CA voltage steps. The good consistency of the data validates the use of LSV polarization data.

Since the ohmic resistance is crucial for the cell operation at higher current

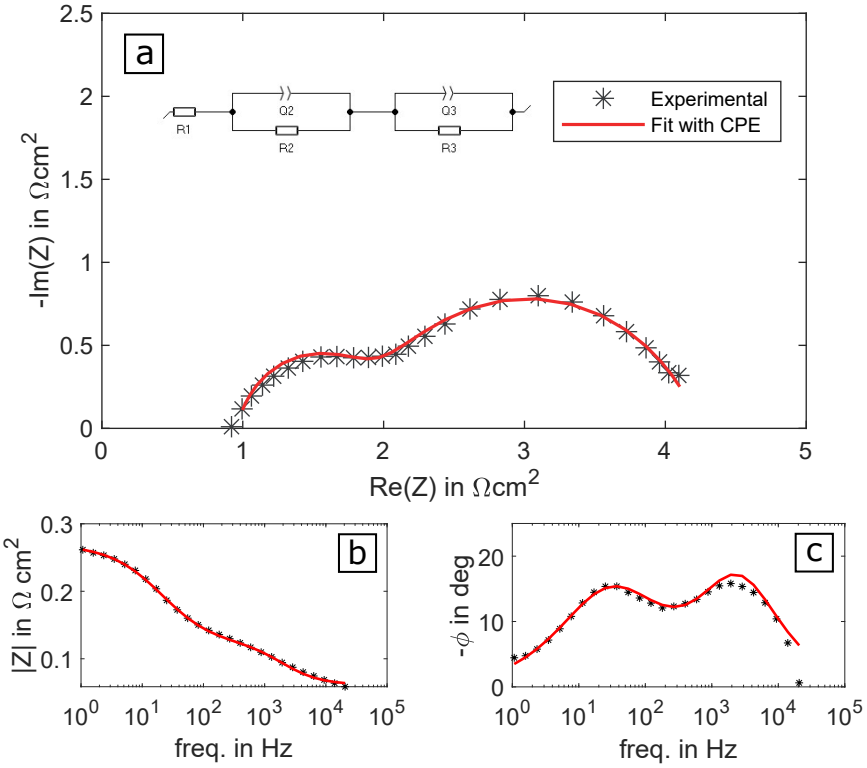

Figure 7: (a)Nyquist plot of the EIS measurement and equivalent circuit model (b)Bode plot of the Impedance and (c) Bode plot of the negative phase shift at 15 mA/cm^2 current density with an amplitude of 1.5 mA/cm^2 from 20 kHz to 1 Hz

densities, the cell ASR was measured with two different methods: ASR_{EIS} values were taken as usual as the high frequency real axis intersections of galvanostatic EIS Nyquist plots as shown in figure 7(a) and ASR_{CI} was determined from current interrupt measurements. The ASR_{EIS} turns out to be 0.96 Ωcm^2 while the $ASR_{CI} = (1.20 \pm 0.03)$ Ωcm^2 (6 repetitions). Increasing the constant current of the galvanostatic EIS measurements did not affect the ASR_{EIS} significantly and resulted in an standard error of 0.01 Ωcm^2. These tubular ASR values are $5 - 6$ times higher than published data for the standard CCM cell approach and can be attributed to the additional longitudinal current conduction length and contact resistances due to a reduced electrode compression on the anode side.

An ASR estimation was determined from the MEA components. Conductivity measurements of the titanium felt exhibit a specific in plane resistance of 2.6 $m\Omega mm$. Considering the diameter of 5 mm, a thickness of 160 μm and a length of 100 mm a theoretical longitudinal inner half cell ASR of 0.84 Ωcm^2 was calculated which is the main contribution the cell ASR. To reduce the half cell resistance, design changes like electrical connection on both sides and increasing the thickness of the titanium felt are necessary and will be considered in the next steps.

In order to gain insight into the half cell contributions, the EIS data shown in figure 7 were additionally analysed by curve fitting of an equivalent circuit model. The equivalent electrical circuits include an ohmic resistance in series with two RQ-components, each consisting of an constant phase element (CPE) and a transfer/activation resistance in parallel and is shown in the top of figure 7(a). The resistance of the RQ-component is related to the charge transfer resistance whereas the CPE is linked to the double layer capacitance. The ohmic resistance R_1 reflects the serial resistance of the membrane and conducting resistances of all components. RQ_2 is assumed to refer to the high frequency relaxation process which is dominated by the HER at the cathode and RQ_3 is assumed to refer to the low frequency relaxation process which is dominated by the OER at the anode[46]. The fitted resistance and capacitance values are

shown in table 1. The root mean square error of $0.0023 \Omega cm^2$ of the fit indicates a good correlation of the fit with the measured impedance.

Table 1: EIS fit results at $i = 15\ mA/cm^2$ ($U = 1.655\ V$)

Paramater	Value
R_1	$0.958\ \Omega cm^2$
R_2	$0.927\ \Omega cm^2$
Q_2	$0.006\ F$
a_2	0.858
R_3	$2.372\ \Omega cm^2$
Q_3	$0.216\ F$
a_3	0.728

R_2 and R_3 can be attributed to the charge transfer resistance and the capacitance of the constant phase element Q_2 and Q_3 can be attributed to the capacitance of the double layer of the cathode and anode. The anodic charge transfer resistance is higher than the cathodic one but of comparable magnitude, which is unusual for PEM electrolysis cells with a platinum loading above $0.1\ mg/cm^2$. The peak at high frequencies shown in the Bode plot of the phase shift in figure 7(c) confirms an influence of the cathode on the cell potential. Thus, efforts for the reduction of the activation overpotential of the tubular PTE cell should consider the anodic and cathodic contributions.

For commercial applications, electrolyzers with multiple cells are needed to reach sufficient system power. While planar cells are stacked and connected by bipolar plates, the aggregation of tubular cells will be in bundles. The electrical and hydraulic connection in these bundles is very flexible compared to a stack of planar cells but will need higher design efforts. Whole cells including the outer current collector of an extruded polymer/graphite compound can be merged in stacks as shown in figure 8 on the right. Due to a low mechanical stability of the polymer/graphite compound compared to stainless steel or titanium, a stack

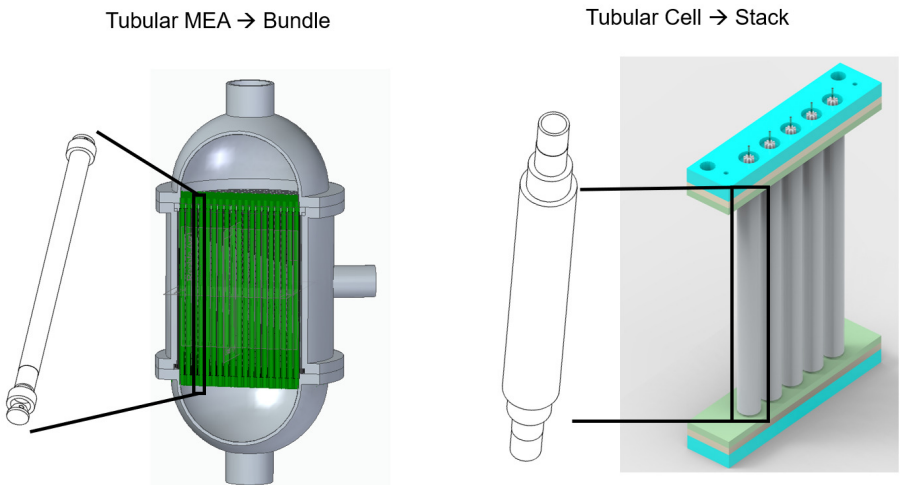

Figure 8: Reactor equipped with tubular MEAs for high pressure PEM electrolysis (left) and Stack design equipped with entire tubular cells for low pressure PEM electrolysis (right)

will be limited to low pressure systems. For high pressure systems, bundles of tubular MEAs enclosed by a reactor shell will be needed as shown in figure 8 on the left.

4. Conclusion and Outlook

This study demonstrates the feasibility of a tubular PEM water electrolysis MEA and cell design and its fabrication process. The tubular approach can lead to production cost reductions due to reduced sealing lengths, an extrusion production and a reduced number of components for the cell assembly. A novel tubular MEA design with a diameter of 5 mm and 100 mm length was fabricated from an extruded tubular membrane and porous transport electrodes. The catalyst was applied by ALD to reach low loadings of 120 $\mu g/cm^2$ iridium on the anode side and 0.28 mg/cm^2 platinum on the cathode side. With the implemented tool for a lab scale fabrication of tubular MEAs, the penetration depth can be defined by the heat bonding parameters time, current and geometric clearance of the pipe and mandrel. The presented MEA design is applicable for an inline fabrication process by lamination of a membrane onto a tubular

PTE. A tubular PEM electrolysis cell using the anodic MEA was operated up to 24 hours at $60C$ without failures of the sealings and electrical connection.

A stable operation of the cell in 1 mol/l sulphuric acid was demonstrated by chronoamperometric steps from 1.2 V to 1.7 V over 12 hours. The observed mass activity of > 680 A/g_{Ir} at $E_{cell} = 1.7$ V is well above literature data though the maximum current density of 55 mA/cm^2 is still low for a commercial application. The performance limitations are attributed to activation overpotentials and ohmic resistances. The analysis of the polarization curve by fitting the Tafel equation shows an exchange current density value of 0.005 mA/cm^2 which is comparable to planar PTE electrodes but a higher Tafel slope of 100 $mV/dec.$ In order to reduce the activation overpotentials, the ALD coating parameters cycle numbers and nano tube dimensions should be optimized. EIS measurements and fits show that the cathode has a large contribution to the activation overpotential which is unusual for the applied platinum loading. A catalyst coating on the membrane as in commercial PEM cells might reduce the contribution of the cathode. The cell ASR of 0.96 Ωcm^2 is about four times higher than in commercial applications and is mainly attributed to the additional, longitudinal, electrical conduction in the inner, anode half cell. Thicker felts, a bidirectional connection or a highly conductive inner structure could be applied to reduce the ASR. Additive manufacturing has the ability to create complex designs and could be used to manufacture tubular titanium substrates according to the needs of electrical conduction and electrolyte transport and is part of the current research.

The limited cell voltage of 1.7 V due to harsh operation conditions in 1 mol/l sulphuric acid leads to a reduced process window and achievable current densities. To increase the process window the operation with much lower acid concentrations or deionised water in combination with an ionomer loading of the PTE is currently investigated. To facilitate a cost effective fabrication of entire cells in a co-extrusion process, conductive copolymers which are already used in tubular vanadium redox flow battery cells, will be considered for the outer cathode half cell. Finally, stack designs with entire tubular cells, includ-

ing the educt and product flow, sealing and electrical connection, are necessary for commercial applications and will be investigated.

5. Acknowledgements

This work was done within the research project Tubulyze and was supported by the German Federal Ministry of Education and Research (BMBF FKZ:03FS0564B).

The authors thank FUMATECH BWT GmbH for pretreatment of the tubular membranes an providing membrane granulate and Rüdiger Schweiss (SGL Carbon GmbH)for the supply with carbon fibre felt research samples.

References

[1] A. Buttler, H. Spliethoff, Current status of water electrolysis for energy storage, grid balancing and sector coupling via power-to-gas and power-to-liquids: A review, Renewable and Sustainable Energy Reviews 82 (2018) 2440–2454. doi:10.1016/j.rser.2017.09.003.

[2] P. Larscheid, L. Lück, A. Moser, Potential of new business models for grid integrated water electrolysis, Renewable Energy 125 (2018) 599–608. doi:10.1016/j.renene.2018.02.074.

[3] S. S. Pethaiah, K. K. Sadasivuni, A. Jayakumar, D. Ponnamma, C. S. Tiwary, G. Sasikumar, Methanol electrolysis for hydrogen production using polymer electrolyte membrane: A mini-review, Energies 13 (22) (2020) 5879. doi:10.3390/en13225879.

[4] D. Besserabov, PEM Electrolysis for Hydrogen Production, Apple Academic Press Inc., 2015.
URL https://www.ebook.de/de/product/24366649/pem_electrolysis_for_hydrogen_production.html

[5] L. Bertuccioli, A. Chan, D. Hart, F. Lehner, B. Madden, E. Standen, Study on developmentof water electrolysis in the eu, Tech. rep., E4tech (Feb. 2014).

[6] D. K. Madheswaran, A. Jayakumar, Recent advancements on non-platinum based catalyst electrode material for polymer electrolyte membrane fuel cells: a mini techno-economic review, Bulletin of Materials Science 44 (4) (nov 2021). doi:10.1007/s12034-021-02572-6.

[7] M. Carmo, D. L. Fritz, J. Mergel, D. Stolten, A comprehensive review on pem water electrolysis, International Journal of Hydrogen Energy 38 (12) (2013) 4901 – 4934. doi:https://doi.org/10.1016/j.ijhydene.2013.01.151.

[8] S. S. Kumar, V. Himabindu, Hydrogen production by PEM water electrolysis – a review, Materials Science for Energy Technologies 2 (3) (2019) 442–454. doi:10.1016/j.mset.2019.03.002.

[9] K. Ayers, The potential of proton exchange membrane–based electrolysis technology, Current Opinion in Electrochemistry 18 (2019) 9–15. doi:10.1016/j.coelec.2019.08.008.

[10] M. Bernt, A. Hartig-Weiß, M. F. Tovini, H. A. El-Sayed, C. Schramm, J. Schröter, C. Gebauer, H. A. Gasteiger, Current challenges in catalyst development for PEM water electrolyzers, Chemie Ingenieur Technik 92 (1-2) (2020) 31–39. doi:10.1002/cite.201900101.

[11] O. Schmidt, A. Gambhir, I. Staffell, A. Hawkes, J. Nelson, S. Few, Future cost and performance of water electrolysis: An expert elicitation study, International Journal of Hydrogen Energy 42 (52) (2017) 30470–30492. doi:10.1016/j.ijhydene.2017.10.045.

[12] C. Minke, M. Suermann, B. Bensmann, R. Hanke-Rauschenbach, Is iridium demand a potential bottleneck in the realization of large-scale PEM wa-

ter electrolysis?, International Journal of Hydrogen Energy 46 (46) (2021) 23581–23590. doi:10.1016/j.ijhydene.2021.04.174.

[13] F. Hegge, F. Lombeck, E. C. Ortiz, L. Bohn, M. von Holst, M. Kroschel, J. Hübner, M. Breitwieser, P. Strasser, S. Vierrath, Efficient and stable low iridium loaded anodes for PEM water electrolysis made possible by nanofiber interlayers, ACS Applied Energy Materials 3 (9) (2020) 8276–8284. doi:10.1021/acsaem.0c00735.

[14] H. Yu, N. Danilovic, Y. Wang, W. Willis, A. Poozhikunnath, L. Bonville, C. Capuano, K. Ayers, R. Maric, Nano-size IrOx catalyst of high activity and stability in PEM water electrolyzer with ultra-low iridium loading, Applied Catalysis B: Environmental 239 (2018) 133–146. doi:10.1016/j.apcatb.2018.07.064.

[15] K. E. Ayers, J. N. Renner, N. Danilovic, J. X. Wang, Y. Zhang, R. Maric, H. Yu, Pathways to ultra-low platinum group metal catalyst loading in proton exchange membrane electrolyzers, Catalysis Today 262 (2016) 121–132. doi:10.1016/j.cattod.2015.10.019.

[16] P. Kúš, A. Ostroverkh, K. Ševčíková, I. Khalakhan, R. Fiala, T. Skála, N. Tsud, V. Matolin, Magnetron sputtered ir thin film on TiC-based support sublayer as low-loading anode catalyst for proton exchange membrane water electrolysis, International Journal of Hydrogen Energy 41 (34) (2016) 15124–15132. doi:10.1016/j.ijhydene.2016.06.248.

[17] T. Hrbek, P. Kúš, Y. Yakovlev, J. Nováková, Y. Lobko, I. Khalakhan, V. Matolín, I. Matolínová, Sputter-etching treatment of proton-exchange membranes: Completely dry thin-film approach to low-loading catalyst-coated membranes for water electrolysis, International Journal of Hydrogen Energy 45 (41) (2020) 20776–20786. doi:10.1016/j.ijhydene.2020.05.245.

[18] Q. Peng, J. S. Lewis, P. G. Hoertz, J. T. Glass, G. N. Parsons, Atomic layer deposition for electrochemical energy generation and storage systems,

Journal of Vacuum Science & Technology A: Vacuum, Surfaces, and Films 30 (1) (2012) 010803. doi:10.1116/1.3672027.

[19] J. Bachmann, Atomic layer deposition, a unique method for the preparation of energy conversion devices, Beilstein Journal of Nanotechnology 5 (2014) 245–248. doi:10.3762/bjnano.5.26.

[20] W.-J. Lee, S. Bera, C. M. Kim, E.-K. Koh, W.-P. Hong, S.-J. Oh, E. Cho, S.-H. Kwon, Synthesis of highly dispersed pt nanoparticles into carbon supports by fluidized bed reactor atomic layer deposition to boost PEMFC performance, NPG Asia Materials 12 (1) (jun 2020). doi:10.1038/s41427-020-0223-x.

[21] S. Schlicht, M. K. S. Barr, M. Wu, P. Hoppe, E. Spiecker, W. Peukert, J. Bachmann, Minimization of catalyst loading on regenerative fuel cell positive electrodes based on titanium felts using atomic layer deposition, ChemElectroChem 5 (24) (2018) 3932–3937. doi:10.1002/celc.201801220.

[22] A. Hofer, S. Bochmann, J. Bachmann, Properties, performance and stability of iridium-coated water oxidation electrodes based on anodized titanium felts, Sustainable Energy and Fuels 5 (2) (2021) 478–485. doi:10.1039/d0se01577f.

[23] A. Laube, A. Hofer, S. Ressel, A. Chica, J. Bachmann, T. Struckmann, PEM water electrolysis cells with catalyst coating by atomic layer deposition (oct 2021). doi:10.1016/j.ijhydene.2021.09.153.

[24] W. Winkler, Brennstoffzellenanlagen, Springer Berlin Heidelberg, 2002. doi:10.1007/978-3-662-06169-5.

[25] W. Dollard, Solid oxide fuel cell developments at westinghouse 37 (1-2) (1992) 133–139. doi:10.1016/0378-7753(92)80070-r.

[26] T. Alston, K. Kendall, M. Palin, M. Prica, P. Windibank, A 1000-cell SOFC reactor for domestic cogeneration 71 (1-2) (1998) 271–274. doi:10.1016/s0378-7753(97)02756-0.

[27] V. Lawlor, S. Griesser, G. Buchinger, A. Olabi, S. Cordiner, D. Meissner, Review of the micro-tubular solid oxide fuel cell 193 (2) (2009) 387–399. doi:10.1016/j.jpowsour.2009.02.085.

[28] S. M. Jamil, M. H. D. Othman, M. A. Rahman, J. Jaafar, A. Ismail, K. Li, Recent fabrication techniques for micro-tubular solid oxide fuel cell support: A review, Journal of the European Ceramic Society 35 (1) (2015) 1–22. doi:10.1016/j.jeurceramsoc.2014.08.034.

[29] A. Tarutin, A. Kasyanova, J. Lyagaeva, G. Vdovin, D. Medvedev, Towards high-performance tubular-type protonic ceramic electrolysis cells with all-ni-based functional electrodes, Journal of Energy Chemistry 40 (2020) 65–74. doi:10.1016/j.jechem.2019.02.014.

[30] M. Yazici, Passive air management for cylindrical cartridge fuel cells 166 (1) (2007) 137–142. doi:10.1016/j.jpowsour.2006.12.085.

[31] B. Bullecks, R. Rengaswamy, D. Bhattacharyya, G. Campbell, Development of a cylindrical PEM fuel cell, International Journal of Hydrogen Energy 36 (1) (2011) 713–719. doi:10.1016/j.ijhydene.2010.09.079.

[32] S. Suseendiran, S. Pearn-Rowe, R. Rengaswamy, Development of cylindrical PEM fuel cells with semi-cylindrical cathode current collectors, International Journal of Hydrogen Energy 45 (17) (2020) 10549–10558. doi:10.1016/j.ijhydene.2019.09.113.

[33] K. I. Lee, S. W. Lee, M. S. Park, C. N. Chu, The development of air-breathing proton exchange membrane fuel cell (PEMFC) with a cylindrical configuration, International Journal of Hydrogen Energy 35 (21) (2010) 11844–11854. doi:10.1016/j.ijhydene.2010.08.105.

[34] T. Park, Y. S. Kang, S. Jang, S. W. Cha, M. Choi, S. J. Yoo, A rollable ultra-light polymer electrolyte membrane fuel cell, NPG Asia Materials 9 (5) (2017) e384–e384. doi:10.1038/am.2017.72.

[35] T. Ward, X. Li, A. Faghri, Performance characteristics of a novel tubular-shaped passive direct methanol fuel cell 196 (15) (2011) 6264–6273. doi:10.1016/j.jpowsour.2011.04.012.

[36] Z.-G. Shao, W.-F. Lin, F. Zhu, P. A. Christensen, H. Zhang, B. Yi, A tubular direct methanol fuel cell with ti mesh anode 160 (2) (2006) 1003–1008. doi:10.1016/j.jpowsour.2006.02.047.

[37] S. Ressel, A. Laube, S. Fischer, A. Chica, T. Flower, T. Struckmann, Performance of a vanadium redox flow battery with tubular cell design, Journal of Power Sources 355 (2017) 199–205. doi:10.1016/j.jpowsour.2017.04.066.

[38] S. Ressel, Tubular all vanadium and vanadium/air redox flow cells, Ph.D. thesis, Universitat Politècnica de València (May 2019).

[39] S. Ressel, P. Kuhn, S. Fischer, M. Jeske, T. Struckmann, An all-extruded tubular vanadium redox flow cell - characterization and model-based evaluation, Journal of Power Sources Advances 12 (2021) 100077. doi:10.1016/j.powera.2021.100077.

[40] S. Schlicht, P. Büttner, J. Bachmann, Highly active ir/TiO2 electrodes for the oxygen evolution reaction using atomic layer deposition on ordered porous substrates, ACS Applied Energy Materials 2 (3) (2019) 2344–2349. doi:10.1021/acsaem.9b00402.

[41] G. Bender, M. Carmo, T. Smolinka, A. Gago, N. Danilovic, M. Mueller, F. Ganci, A. Fallisch, P. Lettenmeier, K. Friedrich, K. Ayers, B. Pivovar, J. Mergel, D. Stolten, Initial approaches in benchmarking and round robin testing for proton exchange membrane water electrolyzers, International

Journal of Hydrogen Energy 44 (18) (2019) 9174–9187. doi:10.1016/j.ijhydene.2019.02.074.

[42] C. Immerz, M. Paidar, G. Papakonstantinou, B. Bensmann, T. Bystron, T. Vidakovic-Koch, K. Bouzek, K. Sundmacher, R. Hanke-Rauschenbach, Effect of the MEA design on the performance of PEMWE single cells with different sizes, Journal of Applied Electrochemistry 48 (6) (2018) 701–711. doi:10.1007/s10800-018-1178-2.

[43] Z. Kang, S. M. Alia, J. L. Young, G. Bender, Effects of various parameters of different porous transport layers in proton exchange membrane water electrolysis, Electrochimica Acta 354 (2020) 136641. doi:10.1016/j.electacta.2020.136641.

[44] K. Bromberger, J. Ghinaiya, T. Lickert, A. Fallisch, T. Smolinka, Hydraulic ex situ through-plane characterization of porous transport layers in PEM water electrolysis cells, International Journal of Hydrogen Energy 43 (5) (2018) 2556–2569. doi:10.1016/j.ijhydene.2017.12.042.

[45] J. Parra-Restrepo, R. Bligny, J. Dillet, S. Didierjean, D. Stemmelen, C. Moyne, A. Degiovanni, G. Maranzana, Influence of the porous transport layer properties on the mass and charge transfer in a segmented PEM electrolyzer, International Journal of Hydrogen Energy 45 (15) (2020) 8094–8106. doi:10.1016/j.ijhydene.2020.01.100.

[46] S. Siracusano, V. Baglio, A. D. Blasi, N. Briguglio, A. Stassi, R. Ornelas, E. Trifoni, V. Antonucci, A. Aricò, Electrochemical characterization of single cell and short stack PEM electrolyzers based on a nanosized IrO2 anode electrocatalyst, International Journal of Hydrogen Energy 35 (11) (2010) 5558–5568. doi:10.1016/j.ijhydene.2010.03.102.